Adaptive demand response with heterogeneous types of thermostatically controlled loads

Xiaoting Chen, Ran Tian, Fanfan Hu, and Simone Baldi, *Senior Member, IEEE*

***Abstract*—When shaping the power consumption of building districts via thermostatically controlled loads (TCLs), it is crucial for demand response programs to consider not only heterogeneity in TCL parameters, but also heterogeneity in the types of TCLs. In this work, we study the feasibility of demand response with heterogeneous types of TCLs and buildings. To study heterogeneity, we create districts consisting of heterogeneous buildings equipped with different thermostatically controlled heating units, air conditioner units, boiler units. The buildings belong to different typologies (light-weight, nearly-zero energy, massive passive), but they all receive the same shift commands on the thermostat set points. Optimality and adaptation of the demand response program are studied analytically in the framework of adaptive linear quadratic control. It is shown that, despite the large heterogeneity, the district power consumption can be regulated by the proposed demand response program, with different types of TCLs serving different tasks, e.g., some units serve coarse regulation of the power consumption, while others serve finer regulation.**

***Index Terms*—Thermostatically controlled loads, heterogeneity, demand response, adaptive linear quadratic control.**

I. Introduction

DUE to their thermal inertia, thermostatically controlled loads (TCLs), comprising air conditioners, boilers, refrigerators, etc., have a huge potential for demand response (DR) [1]. Coordination of TCLs has been studied to provide various services to the power grid, such as frequency regulation, peak shaving, renewable energy integration, and so on [2]–[4]. To support the power balance of the grid, a large amount of TCLs should be involved in the DR program, which however might result in high complexity in the design and implementation of the DR program. A fundamental challenge in the DR field is to construct simple models to manage a large amount of TCLs. This task is not a trivial one, as these models should capture aggregated flexibility despite the inevitable heterogeneity of the loads: not only different parameters, but also different types of TCLs would result in a different dynamic behavior, e.g., the thermostatic behavior of a boiler is different from the thermostatic behavior of an air conditioner. It is hard to obtain system models amenable for optimization and control of heterogeneous TCLs.

Studies have shown that the aggregated power consumption of TCLs may be controlled by properly adjusting their set points: however, these studies most often involve homogeneity assumptions on the TCLs [5]–[8]. Assuming homogeneous TCLs with first-order dynamics, [9] solves a set of Fokker-Planck equations to perform the set point control of TCLs. Fokker-Planck frameworks under homogeneity assumptions also appear in [10], [11], whereas some heterogeneity is considered in [12], [13], by modeling heterogeneity as diffusion noise. To improve the modeling accuracy, [14] studied aggregated power consumption of second-order air and mass temperature dynamics. The approach in [15] uses a deterministic hybrid system to describe individual (homogeneous) load dynamics, and a stochastic hybrid system to capture the aggregated dynamics. Another approach involving stochastic hybrid systems is [16], also relying on homogeneity. Optimization-based approaches have also been studied, where tractability is the main concern [17], [18]: to attain tractability, homogeneous load dynamics are typically assumed. In recent years, distributed control for TCLs has been proposed [19]–[22]: these works obey a different philosophy, with an individual control provided locally to each building, rather than a single control decided centrally by the power provider. These works also rely on some form of homogeneity or regularity of the network, or require local power measurements via smart power sockets. We also refer the reader to a review on modeling options for TCLs [23].

In this work, we depart from the homogeneity perspective. The main contributions of this work are as follows:

- We explore DR programs that can be established even in the presence of large heterogeneity in the buildings and in their TCL equipment. Heterogeneity refers not only to TCLs having different parameters, but also to different types of TCLs and buildings. To this purpose, we consider three main typologies of buildings (lightweight, nearly-zero energy, massive passive), with randomly distributed parameters and subject to different schedules.
- We study optimality and adaptation of the proposed demand response program analytically in the framework of adaptive linear quadratic control. Linear quadratic control is a standard framework for optimal control, whereas adaptation comes from estimation mechanisms to estimate online (from power, set point and weather data) uncertain district parameters.
- We create different districts consisting of heterogeneous buildings equipped with different TCLs (heating units, air conditioner units, boiler units). Extensive numerical experiments show that, despite the large heterogeneity, the district power consumption can be regulated by shifting the thermostat set points. Notably, we verify that different types of TCLs serve different tasks, e.g., some units serve coarse regulation of the consumption, while others serve finer regulation.

This work was partly supported by National Key R&D Program of China grant 2022YFE0198700, and by Natural Science Foundation of China grant 62073074. (Corresponding author: Simone Baldi.)

The authors are with Frontiers Science Center for Mobile Information Communication, School of Mathematics, Southeast University, Nanjing 211189, China (e-mails: {xtchenmath, tr123456202112, zjwzhff0804}@163.com, simonebaldi@seu.edu.cn).

NOMENCLATURE

Main symbols

$T_{\text{zone},i}$	indoor air temperature, zone i
$T^{\text{out}}_{\text{exwall},i}$	external wall outside temperature, zone i
$T^{\text{in}}_{\text{exwall},i}$	external wall inside temperature, zone i
$T_{\text{inwall},i,j}$	inner wall temperature between zones i and j
T_{out}	outdoor ambient temperature
$T_{\text{HR,w}}$	water temperature inside hydronic radiator (HR)
$T_{\text{HR,out}}$	outlet temperature of hydronic radiator
$T_{\text{HR,in}}$	inlet temperature of hydronic radiator
T_{case}	storage tank case temperature
T_{tap}	tap water temperature
C_{exwall}	thermal capacity of the external wall
C_{inwall}	thermal capacity of the inner wall
C_{w}	specific heat capacity of water
C_{a}	specific heat capacity of air
$M_{\text{exwall},i}$	mass of the external wall
$M_{\text{inwall},i,j}$	mass of the inner wall between zones i and j
h_{in}, h_{out}	heat transfer coeff. inside/outside wall surface
h_{case}	convective heat transfer coeff. storage tank case
k_{w}	thermal conductivity of water
α_{loss}	heat loss coefficient of tank
$d_{\text{in}}, d_{\text{out}}$	inner and external diameter of tank
H_{tank}	height of storage tank layer
$A_{\text{exwall},i}$	external wall area, zone i
$A_{\text{inwall},i,j}$	inner wall area between zones i and j
$A_{\text{win},i}$	window area, zone i
A_{HR}	area of hydronic radiator
A_{tank}	cross-section area of storage tank
M_{a}	mass of indoor air
$M_{\text{HR,w}}$	mass of water inside hydronic radiator
M_i	mass of water inside tank, i-th layer
R_{exwall}	thermal resistance of the external wall
R_{win}	thermal resistance of the window
$\dot{m}_{\text{inf}}$	air flow rate due to infiltration
$\dot{m}_{\text{SH}}$	mass flow rate for space heating (SH)
$\dot{m}_{\text{HR}}$	waer flow rate of hydronic radiator
$\dot{m}_{\text{DHW}}$	mass flow rate for domestic hot water (DHW)
G_{out}	outdoor solar radiation
$Q_{\text{SH},i}$	heat gain from space heating
$Q_{\text{HR},i}$	heat gain from hydronic radiator
$Q_{\text{ER},i}$	heat gain from electric radiator (ER)
$Q_{\text{sol},i}$	heat gain from solar radiation
$S_{\text{SH},i}$	on/off status of space heating device
$S_{\text{HR},i}$	on/off status of hydronic radiator
S_{EH}	on/off status of electric heater (EH)
S_{ER}	on/off status of electric radiator
$T^{\text{zone}}_{\text{set}}, T^{\text{tank}}_{\text{set}}$	temperature set point for zone and tank
S_{GSHP}	on/off status of ground source heat pump (GSHP)
$\delta_{\text{zone}}, \delta_{\text{tank}}$	dead-band width of zone and tank

Other abbreviations

TCLs	Thermostatically Controlled Loads
DR	Demand Response
LW	Light Weight (building)
NZ	Nearly-Zero Energy (building)
MP	Massive Passive (building)

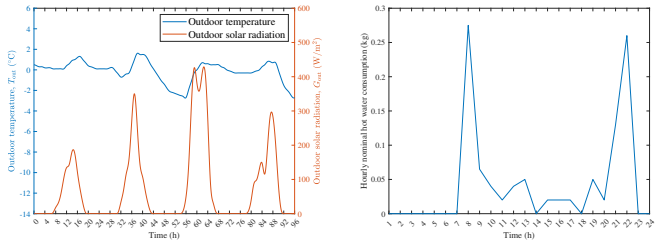

Fig. 1: **Left**: Weather data used in this study; **Right**: Hourly nominal hot water consumption.

To the best of our knowledge, while there are works with heterogeneous TCLs of the same type, we are not aware of any work considering TCLs of different types: partly-related works are [24] considering multi-state TCLs (some control variables are continuous, some are discrete), or [25] considering different types of switching (instantaneous, stochastic), or [26], [27] considering multiple clusters (but clustering TCLs of the same type).

The rest of the work is organized as follows: in Section II, we describe the data used in this study, with the models described in Section III. The design of the DR program is illustrated in Section IV, and stability analysis of the proposed program is in Section V and in the Appendix. Simulations of the district power consumption without DR program are in Section VI, whereas Section VII implements the proposed DR program. Conclusions are drawn in Section VIII.

Notation We adopt a standard notation as follows. For a time signal $y(k)$ collected at discrete time instants k, the notation $\Delta y(k) = y(k+1) - y(k)$ indicates the difference operator, and z represents the forward operator in the Z-transform, i.e. $zy(k) = y(k+1)$. For a square matrix A, its i-th eigenvalue is denoted as $\lambda_i(A)$. Refer to the nomenclature table for symbols adopted in this work.

II. DATA DESCRIPTION

The weather data set used in this work comprise outdoor temperature and solar radiation in one reference year in Helsinki, Finland. We focus on March 16th to 19th, cf. Fig. 1, motivated by the fact that, with low temperature and sufficient solar radiation, the heating demand is relatively high, while the presence of sun increases the flexibility for DR purposes.

To test the implementation of DR programs in a heterogeneous scenario, we create a virtual district with different types of buildings, with different building envelopes and energy systems. The buildings are standard buildings studied in the literature [28]–[30] and belong to three categories: light weight (LW), nearly-zero energy (NZ) and massive passive (MP).

TABLE I: Energy systems in buildings (refer to nomenclature for abbreviations).

	LW	NZ	MP
Zone 1	ER/15kW	HR	HR
Zone 2	ER/15kW	—	HR
Tank, layer 1	EH/4kW	EH/5kW	EH/6kW
Tank, layer 2	—	GSHP/7.5kW	GSHP/8kW

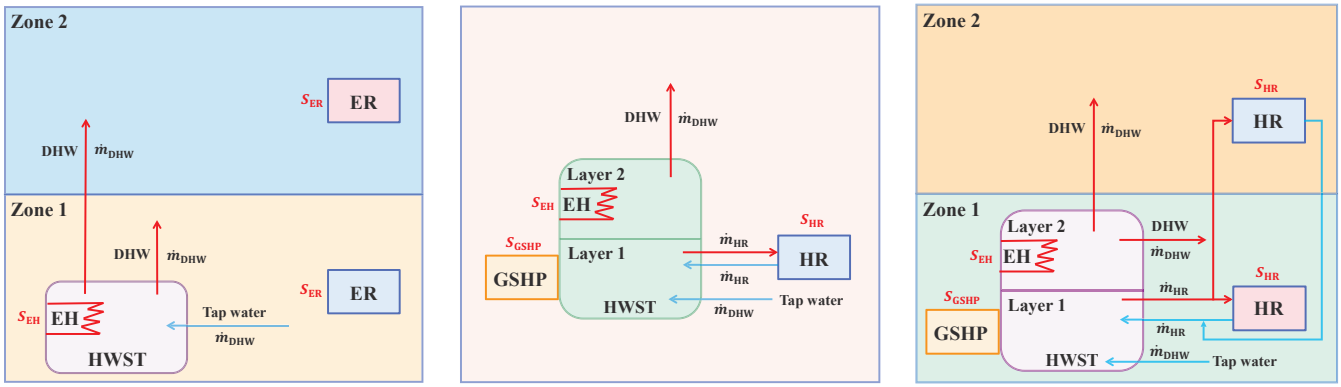

(a) LW building (b) NZ building (c) MP building

Fig. 2: Diagram of TCL connections in different buildings: (a) LW building; (b) NZ building; (c) MP building.

Each building is equipped with domestic hot water and space heating devices, organized as follows and also summarized in Table I, along with the connection of TCLs in the different buildings as illustrated in Fig. 2:

- LW building [28] is a building with poor insulation and airtightness. Domestic hot water is provided by an electric heater inside a single-layer hot water storage tank. Space heating is satisfied by an electric radiator.
- NZ building [29], [30] is a nearly-zero energy building. A double-layer hot water storage tank covers both domestic hot water and space heating demand. An electric heater serves the upper layer of the hot water storage tank, while the lower layer is served by a ground source heat pump. Space heating is delivered by a hydronic radiator.
- MP building [28] is a highly insulated building with large thermal mass and excellent airtightness. The external walls of the building are made of lightweight concrete, while roof and floor are made of massive concrete. The MP building is equipped with similar devices as NZ building, only with different parameters.

To design and implement the DR program, we consider districts with 100 heterogeneous buildings, comprising 33 LW, 33 NZ, and 34 MP buildings. The nominal settings for building parameters, initial and boundary conditions are in Table II. The table is divided into two parts: the first part presents the building envelope parameters, and the second part contains random parameters used to create heterogeneity in the thermal behavior. Uniform random distribution is used to generate the parameters within a specified range. Thus, the different buildings form a heterogeneous population of TCLs. An hourly nominal hot water consumption schedule is defined as in Fig. 1, where the actual hot water consumption in each building is calculated as a random deviation from the nominal schedule.

TABLE II: Nominal values and initial conditions settings.

Description	LW	NZ	MP
U_{exwall} (W/(m^2 K))	0.8	0.17	0.08
U_{roof} (W/(m^2 K))	0.47	0.28	0.07
U_{floor} (W/(m^2 K))	0.35	0.79	0.08
U_{door} (W/(m^2 K))	2.2	1.0	0.5
U_{win} (W/(m^2 K))	2.8	0.7	0.8
Window properties τ_{win}	0.8	0.5	0.5
Airtightness (m^3/hm^2)	7.3	0.4	0.7
No. of occupants	[2, 4]		
Net floor area (m^2)	[63.07, 195]		
Factor of building size	[0.7, 1.3]		
Ground temperature (°C)	[8, 11]		
Zone set point (°C)	[20, 24]		
Tank set point (°C)	[58, 70]		
Hot water consumpt. (kg/h)	[-0.002, 0.277]		

III. Modeling Phase

The models in the district simulator comprise the thermal models of the zones and the hot water storage tank in each building, the model for the thermostatic activation of the corresponding units, and the model for power consumption.

A. Envelope thermal model

1) Indoor temperature dynamics: Indoor temperature dynamics can be captured via the 3R-2C thermal model [31]. This model consists of resistances (R) and capacitances (C) to model the thermal mass of buildings [32]:

$$\begin{aligned} M_{\text{a},i}C_{\text{a}}\dot{T}_{\text{zone},i} &= h_{\text{in}}A_{\text{exwall},i}\left(T^{\text{in}}_{\text{exwall},i} - T_{\text{zone},i}\right) + Q_{\text{ER},i}S_{\text{ER},i} \\ &+ \left(T_{\text{out}} - T_{\text{zone},i}\right)/R_{\text{win},i} + \dot{m}_{\text{inf},i}C_{\text{air}}\left(T_{\text{out}} - T_{\text{zone},i}\right) + Q_{\text{int},i} \\ &+ \sum_j h_{\text{in}}A_{\text{inwall},i,j}\left(T_{\text{inwall},i,j} - T_{\text{zone},i}\right) + Q_{\text{HR},i}S_{\text{HR},i} + Q_{\text{sol},i}, \end{aligned}$$

$$\begin{aligned} 0.5M_{\text{exwall},i}C_{\text{exwall}}\dot{T}^{\text{in}}_{\text{exwall},i} &= h_{\text{in}}A_{\text{exwall},i}\left(T_{\text{zone},i} - T^{\text{in}}_{\text{exwall},i}\right) \\ &+ \left(T^{\text{out}}_{\text{exwall},i} - T^{\text{in}}_{\text{exwall},i}\right)/R_{\text{exwall},i}, \end{aligned}$$

$$\begin{aligned} 0.5M_{\text{exwall},i}C_{\text{exwall}}\dot{T}^{\text{out}}_{\text{exwall},i} &= h_{\text{out}}A_{\text{exwall},i}\left(T_{\text{out}} - T^{\text{out}}_{\text{exwall},i}\right) \\ &+ \left(T^{\text{in}}_{\text{exwall},i} - T^{\text{out}}_{\text{exwall},i}\right)/R_{\text{exwall},i}, \end{aligned}$$

$$\begin{aligned} M_{\text{inwall},i,j}C_{\text{inwall}}\dot{T}_{\text{inwall},i,j} &= h_{\text{in}}A_{\text{inwall},i,j}\left(T_{\text{zone},i} - T_{\text{inwall},i,j}\right) \\ &+ h_{\text{in}}A_{\text{inwall},i,j}\left(T_{\text{zone},j} - T_{\text{inwall},i,j}\right). \end{aligned}$$

The equations describe, for each zone i, the evolution of the indoor air temperature $T_{\text{zone},i}$, the inside and outside wall temperature $T^{\text{in}}_{\text{exwall},i}$, $T^{\text{out}}_{\text{exwall},i}$ and the inner wall temperature $T_{\text{inwall},i,j}$ between zones i and j. Here, $M_{\text{exwall},i}$ and $M_{\text{inwall},i,j}$ (kg) are the mass of the external and inner wall, C_{exwall} and C_{inwall} (J/(kg K)) are the thermal capacity, h_{in} and h_{out} (W/(m^2 K)) are the heat transfer coefficient of the inside and outside surface of the wall, $A_{\text{exwall},i}$ and $A_{\text{inwall},i,j}$ (m^2) are the wall area. T_{out} (°C) is the outdoor ambient

temperature, $M_{\rm a}$ (kg) is the mass of indoor air, $C_{\rm a}$ (J/(kg K)) is the specific heat capacity of air, $R_{\rm exwall} = 1/(A_{{\rm exwall},i}U_{\rm exwall})$ and $R_{\rm win} = 1/(A_{\rm win}U_{\rm win})$ (K/W) are the thermal resistance of the external wall and window, $A_{{\rm win},i}$ is the window area, $\dot{m}_{\rm inf}$ (kg/s) is the air flow rate due to infiltration.

2) Heat gains: The heat gains from electric radiator, hydronic radiator, internal loads are indicated as $Q_{{\rm ER},i}$, $Q_{{\rm HR},i}$, $Q_{{\rm int},i}$ (W), with $S_{{\rm ER},i}$ and $S_{{\rm HR},i}$ being the on/off status of electric and hydronic radiator, which are binary variables, 1 or 0. The heat gain from solar radiation is $Q_{{\rm sol},i}$ (W), expressed as

$$Q_{{\rm sol},i} = \alpha_{{\rm sol},i}\tau_{{\rm win},i}A_{{\rm win},i}G_{\rm out},$$

where $\alpha_{{\rm sol},i}$ is the shading factor, $\tau_{{\rm win},i}$ is the percentage of total solar radiant heat energy transmitted through glazing, $A_{{\rm win},i}$ ($\rm m^2$) denotes area of windows and $G_{\rm out}$ ($\rm W/m^2$) is the outdoor solar radiation. In line with Table I, depending on the type of building, the zone temperature is affected by the electric radiator (in LW building) or by the hydronic radiator (in NZ and MP buildings). If a device is not present in the building, it is understood that its status is always off.

The heat provided by the hydronic radiator can be obtained through the following standard model [33]:

$$\begin{aligned} Q_{\rm HR} &= A_{\rm HR}\left(T_{{\rm HR,w}} - T_{{\rm zone},i}\right)^{2.3}, \\ M_{{\rm HR,w}}C_{\rm w}\dot{T}_{{\rm HR,w}} &= \dot{m}_{\rm HR}A_{\rm HR}C_{\rm w}T_{\rm HR,in} \\ &\quad - \dot{m}_{\rm HR}A_{\rm HR}C_{\rm w}T_{\rm HR,out} - Q_{\rm HR}, \end{aligned}$$

where $T_{\rm HR,w}$ (°C) is the average water temperature inside the radiator, $T_{\rm HR,out}$ and $T_{\rm HR,in}$ (°C) are the outlet and inlet water temperature, where the former is set as 40 °C, and the latter is the same as the water temperature at the outlet of the bottom layer of the tank. $M_{\rm HR,w}$ (kg) is the mass of water inside the radiator, $\dot{m}_{\rm HR}$ (kg/($\rm m^2$ s)) is its flow rate, $A_{\rm HR}$ ($\rm m^2$) is the area of the radiator.

B. Hot Water Storage Tank (HWST) thermal model

The so-called stratified HWST model [33] is considered for describing the storage of thermal energy. In this work, we consider two types of storage tanks, one being a mixed single-layer storage tank, and the other one being a two-layered tank, with high temperature water on top and low temperature at the bottom. The storage tank can be connected to one or more equipment to provide SH or DWH services, refer to the diagrams in Fig. 2.

Considering two tank layers (the single layer case follows accordingly), the energy balance in the tank is as follows:

$$\begin{aligned} 0.5M_1C_{\rm w}\dot{T}_{{\rm tank},1} &= S_{\rm EH}Q_{\rm EH} + \dot{m}_{\rm DHW}C_{\rm w}\left(T_{{\rm tank},2} - T_{{\rm tank},1}\right) \\ &\quad + A_{\rm tank}k_{\rm w}\left(T_{{\rm tank},2} - T_{{\rm tank},1}\right)/H_{\rm tank} \\ &\quad + h_{\rm case}\left(\pi d_{\rm in}H_{\rm tank}\right)\left(T_{\rm case} - T_{{\rm tank},1}\right), \\ 0.5M_2C_{\rm w}\dot{T}_{{\rm tank},2} &= S_{\rm GSHP}Q_{\rm GSHP} + \dot{m}_{\rm DHW}C_{\rm w}T_{\rm tap} \\ &\quad + \dot{m}_{\rm HR}C_{\rm w}T_{\rm HR,out} - \left(\dot{m}_{\rm DHW} + \dot{m}_{\rm HR}\right)C_{\rm w}T_{{\rm tank},2} \\ &\quad + A_{\rm tank}k_{\rm w}\left(T_{{\rm tank},1} - T_{{\rm tank},2}\right)/H_{\rm tank} \\ &\quad + h_{\rm case}\left(\pi d_{\rm in}H_{\rm tank}\right)\left(T_{\rm case} - T_{{\rm tank},2}\right), \\ M_{\rm case}C_{\rm case}\dot{T}_{\rm case} &= -\sum_{i=1}^{2} h_{\rm case}(\pi d_{\rm in}H_{\rm tank})(T_{\rm case} - T_{{\rm tank},i}) \\ &\quad - \alpha_{\rm loss}\left(5\pi d_{\rm out}H_{\rm tank}\right)\left(T_{\rm case} - T_{\rm zone}\right), \end{aligned}$$

TABLE III: Assignment of control variables in different buildings.

LW	NZ	MP
$S_{\rm SH} \to S_{\rm ER}$	$S_{\rm SH} \to S_{\rm HR}$	$S_{\rm SH} \to S_{\rm HR}$
$S_{\rm HWST} \to S_{\rm EH}$	$S_{\rm HWST} \to S_{\rm GSHP}$	$S_{\rm HWST} \to S_{\rm GSHP}$
$T_{\rm tank} \to T_{{\rm tank},1}$	$T_{\rm tank} \to T_{{\rm tank},2}$	$T_{\rm tank} \to T_{{\rm tank},2}$

where $T_{{\rm tank},1}, T_{{\rm tank},2}, T_{\rm case}$ (°C) are the water temperature of the two layers and the case temperature, M_i (kg) is the mass of water inside the i-th layer, $C_{\rm w}$ (J/(kg K)) is the specific heat capacity of water, $\dot{m}_{\rm DHW}$ and $\dot{m}_{\rm HR}$ (kg/s) are the mass flow rate for DHW/HR, $T_{\rm tap}$ (°C) is the tap water temperature, $A_{\rm tank}$ ($\rm m^2$) is the cross-section area of the storage tank, $k_{\rm w}$ (W/(m K)) is the thermal conductivity of water, $h_{\rm case}$ (W/($\rm m^2$ K)) is the convective heat transfer coefficient of the case, $d_{\rm in}$ and $d_{\rm out}$ (m) are the inner and external diameter of the tank, $H_{\rm tank}$ (m) is the height of each layer, $\alpha_{\rm loss}$ (W/($\rm m^2$ K)) is the heat loss coefficient of the tank. The on/off status of electric heater and GSHP are $S_{\rm EH}$ and $S_{\rm GSHP}$, which are binary variables, 1 or 0.

C. Individual and Aggregated TCLs

In line with Table I, the devices to be controlled differ in each building. Accordingly, we define $S_{\rm SH} = S_{\rm ER}, S_{\rm HWST} = S_{\rm EH}$ for LW, $S_{\rm SH} = S_{\rm HR}, S_{\rm HWST} = S_{\rm GSHP}$ for NZ and MP, and also define $T_{\rm tank} = T_{{\rm tank},1}$ for LW, $T_{\rm tank} = T_{{\rm tank},2}$ for NZ and MP, also refer to Table III. Then, the on/off states of the devices are as follows:

$$S_{\rm SH}(k+1) = \begin{cases} 1, & \text{if } T_{\rm zone}(k) \le T_{\rm set}^{\rm zone}(k) - \frac{\delta_{\rm zone}}{2} \\ 0, & \text{if } T_{\rm zone}(k) > T_{\rm set}^{\rm zone}(k) + \frac{\delta_{\rm zone}}{2} \\ S_{\rm SH}(k), & \text{otherwise} \end{cases},$$

$$S_{\rm HWST}(k+1) = \begin{cases} 1, & \text{if } T_{\rm tank}(k) \le T_{\rm set}^{\rm tank}(k) - \frac{\delta_{\rm tank}}{2} \\ 0, & \text{if } T_{\rm tank}(k) > T_{\rm set}^{\rm tank}(k) + \frac{\delta_{\rm tank}}{2} \\ S_{\rm HWST}(k), & \text{otherwise} \end{cases},$$

where k is the discrete time step (taken as 5 minutes in this study), $S_{\rm SH}(k+1)$ and $S_{\rm HWST}(k+1)$ indicate the set points at the next discrete time step, $T_{\rm set}^{\rm zone}$ and $T_{\rm set}^{\rm tank}$ are the temperature set point (thermostatic set point) for zone and tank (which can be time-varying because controlled by the DR program), $\delta_{\rm zone}$ and $\delta_{\rm tank}$ are the dead-band width of the corresponding thermostat (taken as $\delta_{\rm zone}$ = 1 °C and $\delta_{\rm tank}$ = 2 °C). In addition, we have that $S_{\rm EH}$ for NZ and MP buildings follows the rule:

$$S_{\rm EH}(k+1) = \begin{cases} 1, & \text{if } T_{{\rm tank},1}(k) \le 55 \\ 0, & \text{otherwise.} \end{cases}$$

In other words, for the two-layered HWST, we prioritize the use of GSHP, while EH only works when the water temperature of the upper layer falls below a specified minimum temperature (taken as 55 °C).

Then, the normalized aggregated power y of the heterogeneous population of TCLs can be calculated as:

$$y = \frac{\sum_{i,j}\left(Q_{{\rm EH},i}S_{{\rm ER},i} + Q_{{\rm GSHP},i}S_{{\rm GSHP},i} + Q_{{\rm ER},j}S_{{\rm ER},j}\right)}{\sum_{i,j}\left(Q_{{\rm EH},i} + Q_{{\rm GSHP},i} + Q_{{\rm ER},j}\right)}, \tag{1}$$

where normalization is done for better numerical conditioning. Note that hydronic radiators do not contribute to power consumption as they simply transport hot water from the storage tank.

IV. Design of Demand Response Program

The design of the demand response program comprises a parametrization phase in Sect. IV-A (useful to isolate the parameters of interest), a canonical form in Sect. IV-B (to guarantee observability of the system parameters from the measurements of power consumption) and the control design in Sect. IV-C (in the framework of linear quadratic control). In the following, we provide the details of the different steps.

A. Parametrization phase

In order to model the evolution of the power consumption in the district, let us consider autoregressive moving average model as follows:

$$\begin{aligned} y(k) = &- a_1 y(k-1) + b_1 T_{\text{set}}^{\text{zone}}(k-1) + b_2 T_{\text{set}}^{\text{zone}}(k-2) \\ &+ b_3 T_{\text{set}}^{\text{zone}}(k-3) + c_1 T_{\text{set}}^{\text{tank}}(k-1) + c_2 T_{\text{set}}^{\text{tank}}(k-2) \\ &+ c_3 T_{\text{set}}^{\text{tank}}(k-3) + d_1 T_{\text{out}}(k-1) + d_2 T_{\text{out}}(k-2) \\ &+ f_1 G_{\text{out}}(k-1) + g, \end{aligned} \tag{2}$$

where y is the normalized aggregrated power as in (1). The parameters $a_1,\ b_1,\ \dots\ ,\ g$ describe the evolution of the aggregrated power as a function of the variables $T_{\text{set}}^{\text{zone}}$, $T_{\text{set}}^{\text{tank}}$, T_{out} and G_{out}, which are all averaged within one time step. It can be noted that the power consumption is taken to depend on the outside temperature T_{out} and solar radiation G_{out}, as it will be verified in Sect. VI.

Let us denote the power tracking error as

$$e(k) = y(k) - y_d(k), \tag{3}$$

where y_d is a piecewise constant reference normalized aggregrated power. Filtering each side of (2) with $(1 - z^{-1})$ and using (3), we obtain

$$\begin{aligned} (1-z^{-1})e(k) = (1-z^{-1})[&-a_1 y(k-1) + b_1 T_{\text{set}}^{\text{zone}}(k-1) \\ &+ b_2 T_{\text{set}}^{\text{zone}}(k-2) + b_3 T_{\text{set}}^{\text{zone}}(k-3) + c_1 T_{\text{set}}^{\text{tank}}(k-1) \\ &+ c_2 T_{\text{set}}^{\text{tank}}(k-2) + c_3 T_{\text{set}}^{\text{tank}}(k-3) + d_1 T_{\text{out}}(k-1) \\ &+ d_2 T_{\text{out}}(k-2) + f_1 G_{\text{out}}(k-1) + g]. \end{aligned}$$

We get the error dynamics

$$\begin{aligned} e(k) = &\ a_{1d} e(k-1) + a_{2d} e(k-2) + b_1 \Delta T_{\text{set}}^{\text{zone}}(k-1) \\ &+ b_2 \Delta T_{\text{set}}^{\text{zone}}(k-2) + b_3 \Delta T_{\text{set}}^{\text{zone}}(k-3) + c_1 \Delta T_{\text{set}}^{\text{tank}}(k-1) \\ &+ c_2 \Delta T_{\text{set}}^{\text{tank}}(k-2) + c_3 \Delta T_{\text{set}}^{\text{tank}}(k-3) + d_1 \Delta T_{\text{out}}(k-1) \\ &+ d_2 \Delta T_{\text{out}}(k-2) + f_1 \Delta G_{\text{out}}(k-1), \end{aligned} \tag{4}$$

where $a_{1d} = 1 - a_1,\ a_{2d} = a_1$, and $\Delta T_{\text{set}}^{\text{zone}}(k)$, $\Delta T_{\text{set}}^{\text{tank}}(k)$ are the temperature set point shift for zone and tank. The dynamics (4) can be rewritten in the linear parametric form

$$\zeta(k) = \boldsymbol{\theta}^{*\top} \boldsymbol{\Phi}(k), \tag{5}$$

where $\zeta(k) = e(k)$ and

$$\boldsymbol{\theta}^* = [b_1 \ \ b_2 \ \ b_3 \ \ c_1 \ \ c_2 \ \ c_3 \ \ d_1 \ \ d_2 \ \ f_1 \ \ a_{1d} \ \ a_{2d}]^\top,$$

$$\begin{aligned} \boldsymbol{\Phi}(k) = \big[&\Delta T_{\text{set}}^{\text{zone}}(k-1) \ \ \Delta T_{\text{set}}^{\text{zone}}(k-2) \ \ \Delta T_{\text{set}}^{\text{zone}}(k-3) \\ &\Delta T_{\text{set}}^{\text{tank}}(k-1) \ \ \Delta T_{\text{set}}^{\text{tank}}(k-2) \ \ \Delta T_{\text{set}}^{\text{tank}}(k-3) \\ &\Delta T_{\text{out}}(k-1) \ \ \Delta T_{\text{out}}(k-2) \ \ \Delta G_{\text{out}}(k-1) \\ &e(k-1) \ \ e(k-2)\big]^\top. \end{aligned}$$

Due to the large heterogeneity of the dynamics, the parameters in $\boldsymbol{\theta}^*$ are unknown and must be estimated from data. The estimation law we consider is based on the recursive least-squares algorithm [34]:

$$\varepsilon(k) = \frac{\zeta(k) - \boldsymbol{\theta}^\top(k-1)\boldsymbol{\Phi}(k)}{m^2(k)}, \tag{6}$$

$$m^2(k) = 1 + \alpha \boldsymbol{\Phi}^\top(k)\boldsymbol{\Phi}(k) + \boldsymbol{\Phi}^\top(k) P_1 \boldsymbol{\Phi}(k), \tag{7}$$

$$\boldsymbol{\theta}(k) = \boldsymbol{\theta}(k-1) + P_1(k)\boldsymbol{\Phi}(k)\varepsilon(k), \tag{8}$$

$$P_1(k) = \frac{1}{\beta}\left(P_1(k-1) - \frac{P_1(k-1)\boldsymbol{\Phi}(k)\boldsymbol{\Phi}^\top(k)P_1(k-1)}{m^2(k)\beta + \boldsymbol{\Phi}^\top(k)P_1(k-1)\boldsymbol{\Phi}(k)}\right), \tag{9}$$

where $\varepsilon(k)$ is the estimation error, $m(k) > 0$ is a normalization signal satisfying $\|P_1(k)\|\boldsymbol{\Phi}^2(k)/m^2(k) < 2$, $P_1(k) = P_1(k)^\top > 0$ is the adaptive gain, and α, β are nonnegative design constants representing a normalizing factor and a forgetting factor, respectively.

B. Observable canonical form

Controllability and observability properties are important in demand response [35]. The purpose of this section is to make sure that the system parameters are observable through the tracking error in (3). This is possible using an observable canonical form for the system dynamics.

***Definition** 1:* (**Observable canonical form** [34]) For a general nth order transfer function:

$$H(z) = \frac{q_{n-1}z^{n-1} + \cdots + q_1 z + q_0}{z^n + p_{n-1}z^{n-1} + \cdots + p_1 z + p_0},$$

the observable canonical state-space form is

$$\boldsymbol{x}(k+1) = A\boldsymbol{x}(k) + Bu(k), \quad y(k) = C^\top \boldsymbol{x}(k),$$

with

$$A = \begin{bmatrix} -p_{n-1} & 1 & 0 & \cdots & 0 \\ -p_{n-2} & 0 & 1 & \cdots & 0 \\ \vdots & \vdots & & \ddots & \\ -p_1 & 0 & 0 & \cdots & 1 \\ -p_0 & 0 & 0 & \cdots & 0 \end{bmatrix}, \ B = \begin{bmatrix} q_{n-1} \\ q_{n-2} \\ \vdots \\ q_1 \\ q_0 \end{bmatrix},$$

$$C = [1 \ \ 0 \ \ \cdots \ \ 0 \ \ 0]^\top.$$

To obtain an observable canonical form for the district, let us first use (4) to obtain the following state-space model

$$\begin{aligned} \boldsymbol{x_d}(k+1) &= A_d \boldsymbol{x_d}(k) + [B_{d,1} \ \ B_{d,2}]\Delta \boldsymbol{T_{\text{set}}}(k), \\ e(k) &= C_d^\top \boldsymbol{x_d}(k), \end{aligned} \tag{10}$$

with

$$\begin{aligned} \boldsymbol{x_d}(k) = [&\Delta T_{\text{set}}^{\text{zone}}(k-2) \ \ \Delta T_{\text{set}}^{\text{zone}}(k-1) \ \ \Delta T_{\text{set}}^{\text{tank}}(k-2) \\ &\Delta T_{\text{set}}^{\text{tank}}(k-1) \ \ \Delta T_{\text{out}}(k-1) \ \ \Delta T_{\text{out}}(k) \\ &\Delta G_{\text{out}}(k) \ \ e(k-1) \ \ e(k)]^\top, \end{aligned}$$

$$\Delta \boldsymbol{T_{\text{set}}}(k) = [\Delta T_{\text{set}}^{\text{zone}}(k) \ \ \Delta T_{\text{set}}^{\text{tank}}(k)]^\top,$$

$$A_d = \begin{bmatrix} 0 & 1 & 0 & 0 & 0 & 0 & 0 & 0 & 0 \\ 0 & 0 & 0 & 0 & 0 & 0 & 0 & 0 & 0 \\ 0 & 0 & 0 & 1 & 0 & 0 & 0 & 0 & 0 \\ 0 & 0 & 0 & 0 & 0 & 0 & 0 & 0 & 0 \\ 0 & 0 & 0 & 0 & 0 & 1 & 0 & 0 & 0 \\ 0 & 0 & 0 & 0 & 0 & 1 & 0 & 0 & 0 \\ 0 & 0 & 0 & 0 & 0 & 0 & 1 & 0 & 0 \\ 0 & 0 & 0 & 0 & 0 & 0 & 0 & 0 & 1 \\ b_3 & b_2 & c_3 & c_2 & d_2 & d_1 & f_1 & a_{2d} & a_{1d} \end{bmatrix},$$

$$B_{d,1} = [0 \ 1 \ 0 \ 0 \ 0 \ 0 \ 0 \ 0 \ b_1]^\top,$$

$$B_{d,2} = [0 \ 0 \ 0 \ 1 \ 0 \ 0 \ 0 \ 0 \ c_1]^\top,$$

$$C_d = [0 \ 0 \ 0 \ 0 \ 0 \ 0 \ 0 \ 0 \ 1]^\top.$$

From the superposition principle, the tracking error is obtained from

$$e = H_1(z)\Delta T_{\text{set}}^{\text{zone}} + H_2(z)\Delta T_{\text{set}}^{\text{tank}}, \tag{11}$$

where

$$H_1(z) \triangleq C_d^\top (zI - A_d)^{-1} B_{d,1} = \frac{b_1 z^2 + b_2 z + b_3}{z^3 - a_{1d} z^2 - a_{2d} z}, \tag{12}$$

$$H_2(z) \triangleq C_d^\top (zI - A_d)^{-1} B_{d,2} = \frac{c_1 z^2 + c_2 z + c_3}{z^3 - a_{1d} z^2 - a_{2d} z}. \tag{13}$$

Let us express the transfer functions (12), (13) as

$$H_1(z) = \frac{Z_{q,1}(z)}{R_p(z)}, \ H_2(z) = \frac{Z_{q,2}(z)}{R_p(z)}, \tag{14}$$

where

$$R_p(z) = z^3 + \boldsymbol{\theta}_p^{*\top} \bar{\boldsymbol{\alpha}}(z), \ \boldsymbol{\theta}_p^* = [-a_{1d} \ -a_{2d} \ 0]^\top,$$
$$Z_{q,1}(z) = \boldsymbol{\theta}_{q,1}^{*\top} \bar{\boldsymbol{\alpha}}(z), \ \boldsymbol{\theta}_{q,1}^* = [b_1 \ b_2 \ b_3]^\top,$$
$$Z_{q,2}(z) = \boldsymbol{\theta}_{q,2}^{*\top} \bar{\boldsymbol{\alpha}}(z), \ \boldsymbol{\theta}_{q,2}^* = [c_1 \ c_2 \ c_3]^\top,$$

and $\boldsymbol{\theta}_p^*, \ \boldsymbol{\theta}_{q,1}^*, \ \boldsymbol{\theta}_{q,2}^* \in \mathbb{R}^3$ are the coefficient vectors of the corresponding polynomials and $\bar{\boldsymbol{\alpha}}(z) = [z^2 \ z \ 1]^\top$.

The system (11) can be equivalently rewritten in its observable canonical form:

$$\boldsymbol{x}(k+1) = A\boldsymbol{x}(k) + B\Delta \boldsymbol{T}_{\mathbf{set}}(k), \ e(k) = C^\top \boldsymbol{x}(k), \tag{15}$$

where $x \in \mathbb{R}^3$ and

$$A = \left[\begin{array}{c} -\boldsymbol{\theta}_p^* \\ \hline \begin{array}{ccc} & I_2 & \\ 0 & & \end{array} \end{array}\right], \ B = \left[\boldsymbol{\theta}_{q,1}^* \quad \boldsymbol{\theta}_{q,2}^*\right], \ C = [1 \ 0 \ 0]^\top. \tag{16}$$

The canonical form (15)-(16) can be used for stability analysis.

C. Optimal and adaptive control

It is well known that linear quadratic control is the most standard approach to optimal control [34], [36]. In our application, optimal control is defined via the quadratic objective function

$$J = \sum_{k=0}^{\infty} [\boldsymbol{x}^\top(k) Q \boldsymbol{x}(k) + \Delta \boldsymbol{T}_{\mathbf{set}}{}^\top(k) R \Delta \boldsymbol{T}_{\mathbf{set}}(k)] \tag{17}$$

expressing a trade-off between power tracking error (i.e. energy consumption) and set point shifts (i.e. users' flexibility). This trade-off is regulated via the positive definite matrices Q and R.

The control objective of the demand response program is as follows:

Control Objective: Design the set point shifts $\Delta T_{\text{set}}^{\text{zone}}(k)$ and $\Delta T_{\text{set}}^{\text{tank}}(k)$ so that $e(k)$ converges to zero, i.e. the normalized aggregrated power of the TCL group $y(k)$ tracks the reference power $y_d(k)$ as k goes to ∞ by minimizing the quadratic cost function (17).

For a system in the form of (15), the optimal control law takes the form

$$\Delta \boldsymbol{T}_{\mathbf{set}}(k) = -K\boldsymbol{x}(k), \tag{18}$$

with feedback gain

$$K = (B^\top P B + R)^{-1} B^\top P A, \tag{19}$$

where P is the solution of the Riccati equation:

$$P = A^\top P A - (A^\top P B)(B^\top P B + R)^{-1}(B^\top P A) + Q. \tag{20}$$

In other words, by obtaining the district dynamics in the form (15), the controller (18) allows to implement a demand response program for the district. However, due to the presence of unknown coefficients in the matrices A, B, (19)-(20) cannot be implemented directly, and one should consider an adaptive version of linear quadratic control

$$K = (\hat{B}^\top P \hat{B} + R)^{-1} \hat{B}^\top P \hat{A}, \tag{21}$$

$$P = \hat{A}^\top P \hat{A} - (\hat{A}^\top P \hat{B})(\hat{B}^\top P \hat{B} + R)^{-1}(\hat{B}^\top P \hat{A}) + Q, \tag{22}$$

with $\hat{A}$, $\hat{B}$ the estimated matrices of A and B in (16), respectively,

$$\hat{A} = \left[\begin{array}{c} -\boldsymbol{\theta}_p \\ \hline \begin{array}{ccc} & I_2 & \\ 0 & & \end{array} \end{array}\right], \ \hat{B} = \left[\boldsymbol{\theta}_{q,1} \quad \boldsymbol{\theta}_{q,2}\right], \tag{23}$$

where

$\boldsymbol{\theta}_p \triangleq [-\hat{a}_{1d} \ -\hat{a}_{2d} \ 0]^\top$, $\boldsymbol{\theta}_{q,1} \triangleq [\hat{b}_1 \ \hat{b}_2 \ \hat{b}_3]^\top$, $\boldsymbol{\theta}_{q,2} \triangleq [\hat{c}_1 \ \hat{c}_2 \ \hat{c}_3]^\top$, and the parameters being estimated through (6)-(9). We then obtain an adaptive version of the demand response program that can deal with unknown system parameters.

V. Stability Analysis of Demand Response Program

This section provides the stability analysis for the proposed demand response program. As compared to existing adaptive and optimal controllers, including results by some of the authors [36], the importance of the presented stability analysis is that the different set points for space heating and tank require multi-input single-output analysis, more challenging than single-input single-output analysis. Also, the exogenous weather conditions are explicitly included in the dynamics via the observable canonical form (10). After a few preliminary definitions in Sect. V-A, we first address the known parameter case in Sect. V-B, and then the unknown parameter case in Sect. V-C.

A. Preliminary definitions

The following definitions are instrumental to stability analysis.

Definition 2: (**ℓ_2 norm, ℓ_∞ norm** [34]) The ℓ_2 norm of a discrete-time signal $x(\cdot)$ is defined as

$$\|x\|_2 \triangleq \left(\sum_{s=0}^{\infty} x^\top(s) x(s)\right)^{1/2},$$

and the ℓ_∞ norm of a discrete-time signal $x(\cdot)$ is defined as

$$\|x\|_\infty \triangleq \sup_{s \geq 0} \left(x^\top(s) x(s)\right)^{1/2}.$$

We say that $x \in \ell_2$ (respectively, $x \in \ell_\infty$) if $\|x\|_2$ (respectively, $\|x\|_\infty$) exists. Recall that, for discrete-time signals, $x \in \ell_2 \iff x \in \ell_2 \cap \ell_\infty$.

Definition 3: (**$\ell_{2\delta}$ norm** [34]) For any discrete-time signal $x : \mathbb{Z}^+ \to \mathbb{R}$, x_k denotes the truncation of x to the discrete-time interval $[0, k]$

$$x_k(s) = \begin{cases} x(s), & \text{if } s \le k \\ 0, & \text{otherwise.} \end{cases}$$

The exponentially weighted ℓ_2 norm of x_k is defined as

$$\|x_k\|_{2\delta} \triangleq \left(\sum_{s=0}^{k} \delta^{k-s} x^\top(s) x(s) \right)^{1/2},$$

with $0 < \delta \le 1$. We say that $x \in \ell_{2\delta}$ if $\|x_k\|_{2\delta}$ exists.

B. Stability analysis for known parameter case

The following stability result holds.

Theorem 1: Consider the district system (10)-(14) with $R_p(z)$ coprime to $Z_{q,1}(z)$ and $Z_{q,2}(z)$, and the performance cost (17) where $Q \ge 0$, $R > 0$ are design matrices with Q chosen as $Q = CC^\top$. Consider further the control law

$$\Delta \boldsymbol{T}_{\mathbf{set}}(k) = -K\hat{\boldsymbol{x}}(k), \; K = (B^\top P B + R)^{-1} B^\top P A, \tag{24}$$

$$\hat{\boldsymbol{x}}(k+1) = A\hat{\boldsymbol{x}}(k) + B\Delta \boldsymbol{T}_{\mathbf{set}}(k) - K_o(C^\top \hat{\boldsymbol{x}}(k) - e(k)), \tag{25}$$

where $P = P^\top > 0$ satisfies the discrete-time algebraic Riccati equation (20) and K_o chosen to assign the eigenvalues of $A - K_o C^\top$ to the zeros of a user-defined Hurwitz polynomial of degree 3 $A_o^*(z)$, i.e. $\det(zI - A + K_o C^\top) = A_o^*(z)$. Then, it is guaranteed that all closed-loop signals are bounded, and that $e(k)$ converges to 0 exponentially as k goes to ∞.

Proof: See the Appendix A. □

C. Stability analysis for unknown parameter case

The following properties of the estimation law are useful for stability analysis.

Lemma 1: ([34]) For a linear parametric model as in (5), the estimation law (6)-(9) exhibits the following properties:

(i) $\boldsymbol{\theta}(k) \in \ell_\infty$.
(ii) $\varepsilon(k), \varepsilon(k)m(k), \varepsilon(k)\boldsymbol{\Phi}(k), |\boldsymbol{\theta}(k) - \boldsymbol{\theta}(k-N)| \in \ell_2 \cap \ell_\infty$.
(iii) $\varepsilon(k), \varepsilon(k)m(k), |\varepsilon(k)\boldsymbol{\Phi}(k)|, |\boldsymbol{\theta}(k) - \boldsymbol{\theta}(k-N)| \to 0$ as $k \to \infty$, with any finite integer $N \ge 1$.

Let us define the polynomials

$$\hat{R}_p(z,k) = z^3 + \boldsymbol{\theta}_p^\top(k)\bar{\boldsymbol{\alpha}}(z), \; \hat{Z}_{q,1}(z,k) = \boldsymbol{\theta}_{q,1}^\top(k)\bar{\boldsymbol{\alpha}}(z),$$

$$\hat{Z}_{q,2}(z,k) = \boldsymbol{\theta}_{q,2}^\top(k)\bar{\boldsymbol{\alpha}}(z),$$

with $\boldsymbol{\theta}_p$, $\boldsymbol{\theta}_{q,1}$, $\boldsymbol{\theta}_{q,2}$ as in (23). The following stability result holds.

Theorem 2: Consider the district system (10)-(14) with the estimation mechanism (6)-(9), and let the polynomial $\hat{R}_p(z,k)$ be strongly coprime to $\hat{Z}_{q,1}(z,k)$ and $\hat{Z}_{q,2}(z,k)$ at each time k. Consider further the adaptive control scheme described by the estimation law (6)-(9) and the control

$$\begin{aligned} \Delta \boldsymbol{T}_{\mathbf{set}}(k) &= -\hat{K}(k)\hat{\boldsymbol{x}}(k), \\ \hat{K}(k) &= \left(\hat{B}^\top(k)P(k)\hat{B}(k) + R\right)^{-1} \hat{B}^\top(k)P(k)\hat{A}(k), \\ \hat{\boldsymbol{x}}(k+1) &= \hat{A}(k)\hat{\boldsymbol{x}}(k) + \hat{B}(k)\Delta \boldsymbol{T}_{\mathbf{set}}(k) \\ &\quad - \hat{K}_o(k)\big(C^\top \hat{\boldsymbol{x}}(k) - e(k)\big), \end{aligned} \tag{26}$$

with $\hat{A}$, $\hat{B}$ as in (23) and

$$\hat{K}_o(k) = \boldsymbol{p}^* - \boldsymbol{\theta}_p(k) \tag{27}$$

chosen to assign the eigenvalues of $\hat{A}(k) - \hat{K}_o(k)C^\top$ to the zeros of a given Hurwitz polynomial $A_o^*(z)$, i.e. $\det(zI - \hat{A}(k) + \hat{K}_o(k)C^\top) = A_o^*(z)$, with $\boldsymbol{p}^*$ the coefficient vector of $A_o^*(z) - z^3$, and $P(k)$ resulting from the following Riccati difference equation

$$\begin{aligned} P(k+1) = \hat{A}^\top(k)P(k)\hat{A}(k) + Q - \hat{A}^\top(k)P(k)\hat{B}(k) \\ \left(\hat{B}^\top(k)P(k)\hat{B}(k) + R\right)^{-1} \hat{B}^\top(k)P(k)\hat{A}(k), \end{aligned}$$

with initial condition $P(0) = Q$. Then, it is guaranteed that all closed-loop signals are bounded and the regulation error $e(k)$ converges to zero as k goes to ∞.

Proof: See the Appendix B. □

VI. District Power Consumption with nominal operation

In this section, we aim to show the effect of input variables (thermostat set point deviations $\Delta T_{\text{set}}^{\text{zone}}$ and $\Delta T_{\text{set}}^{\text{tank}}$) and exogenous variables (outdoor temperature T_{out}, solar radiation G_{out}) on the aggregated power. We take zone set points and storage tank set points as $T_{\text{set}}^{\text{zone}} = 22$ °C and $T_{\text{set}}^{\text{tank}} = 64$ °C for all buildings. Then, we consider two scenarios:

- Nominal (uncontrolled) scenario: here, $\Delta T_{\text{set}}^{\text{zone}} = 0$, $\Delta T_{\text{set}}^{\text{tank}} = 0$;
- Open-loop scenario: here, predefined stepwise profiles for $\Delta T_{\text{set}}^{\text{zone}}$ and $\Delta T_{\text{set}}^{\text{tank}}$.

The results from the corresponding scenarios are in Fig. 3, where we have separated the power consumption for space heating (y_{SH} in yellow) from the power consumption of the tank (y_{HWST} in blue). One can notice that the latter is smaller due to the higher efficiency of the GSHP. The set point shifts $\Delta T_{\text{set}}^{\text{zone}}$ and $\Delta T_{\text{set}}^{\text{tank}}$ are represented in red. Fig. 3 contains several lines because five different realizations are provided: this is done to show the consistency of the district simulator.

To better appreciate the difference between the power consumption in the nominal scenario and in the open-loop scenario, refer to Fig. 3c: it can be seen that deviating the set points has a significant effect on the power consumption, both in terms of increase and decrease. It is worth mentioning that the power consumption is not stationary, which reflects the influence of the weather conditions (outdoor temperature T_{out}, solar radiation G_{out}) on the power consumption. Indeed, by comparing Fig. 3c with Fig. 1, one can notice that the peaks of power consumption correspond to the valleys in outdoor temperature, whereas the valleys in power consumption are induced by high solar radiation and high outdoor temperature (which is reasonable in a heating scenario). This justifies the use of T_{out} and G_{out} in the district model (10)-(14). Fig. 3c shows that raising the set point increases power consumption, while lowering the set point reduces it, which again is reasonable in a heating scenario. Let us also remark on the fact that the noisy profiles in Fig. 3c are an inevitable effect of the heterogeneity in the TCLs and buildings. This reflects a realistic power consumption in a district where the actual district dynamics are more complex than (10)-(14), and it is practically impossible to remove the noise and achieve perfect power tracking. Such noisy profiles can be attenuated, but not eliminated by control.

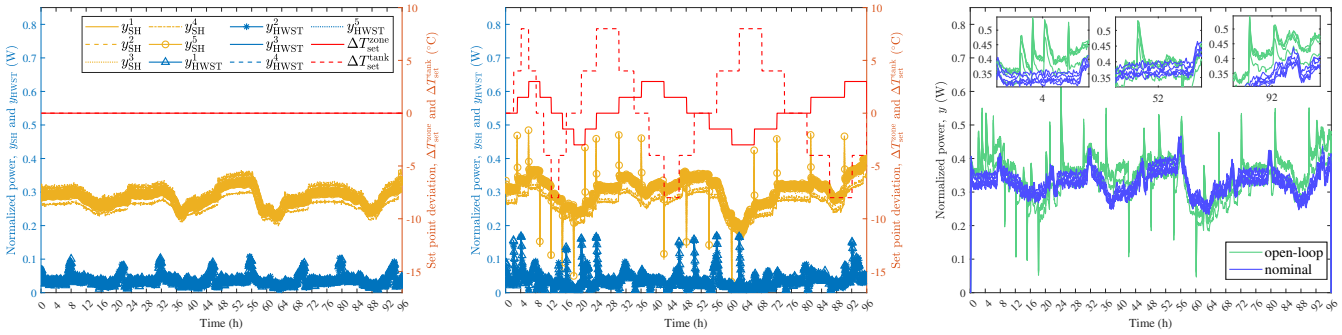

(a) Nominal (uncontrolled) scenario. (b) Open-loop scenario. (c) Comparison for the two scenarios.

Fig. 3: Aggregated TCLs power y in different scenarios: (a) Nominal (uncontrolled) scenario; (b) Open-loop scenario (with predefined stepwise $\Delta T_{\text{set}}^{\text{zone}}$ and $\Delta T_{\text{set}}^{\text{tank}}$). The figures report different experiments from five randomly generated datasets, separated into space heating consumption y_{SH} (in yellow) and hot water storage tank consumption y_{HWST} (in blue). (c) Comparison between nominal and open-loop scenarios: set points shifts ($\Delta T_{\text{set}}^{\text{zone}}$ and $\Delta T_{\text{set}}^{\text{tank}}$) affect the aggregated power.

VII. District Power Consumption with Demand Response

The goal is to make the normalized aggregated average power of TCLs y track a desired value y_d. We choose three values $y_d = \{0.32, 0.35, 0.38\}$, where the value 0.35 has been selected as it is roughly the average of the normalized power reported in Fig 3c, the other two values represent a 3% decrease and 3% increase.

The control architecture for the DR program is sketched in Fig 4. The control signals (deviation for zone and tank set point) are the same for all buildings and decided by a central controller, as common practice in DR programs: the controller takes as feedback the power y collected among all buildings in the district.

To show the feasibility of controlling the district despite all its heterogeneities, we adopt three types of DR programs for comparison:

(1) PID control,
(2) LQC, non-adaptive linear quadratic control,
(3) ALQC, adaptive linear quadratic control (proposed).

The reasons why these methods have been selected are as follows: PID control is arguably the common practice in TCL control; tests with non-adaptive control are important to show the role of uncertainty in performance degradation of the demand response. The PID strategy takes the form

$$\begin{aligned}\Delta T_{\text{set}}^{\text{zone}}(k+1) &= \Delta T_{\text{set}}^{\text{zone}}(k) + K_p^1 e(k) + K_d^1 \Delta e(k)\\ \Delta T_{\text{set}}^{\text{tank}}(k+1) &= \Delta T_{\text{set}}^{\text{tank}}(k) + K_p^2 e(k) + K_d^2 \Delta e(k)\end{aligned} \tag{28}$$

where the PID gains are choosen as

$$K_p^1 = -2.68,\ K_d^1 = -0.38,\ K_p^2 = -3.80,\ K_d^2 = -0.62,$$

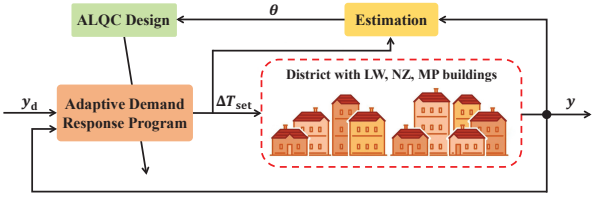

Fig. 4: Diagram of DR program with proposed ALQC. Because the set point shifts are decided centrally by the power provider, they are equally applied to all buildings.

which have been tuned by trial and error.

The comparisons are performed in three heterogeneously generated districts with four settings for y_d:

- three levels of $y_d = \{0.32, 0.35, 0.38\}$,
- piecewise y_d, changing in a stepwise fashion among the three levels of y_d.

The total costs, calculated according to the objective function (17), are summarized in Table IV for different DR programs and scenarios.

It can be observed from Table IV that the proposed ALQC has the least total cost among the three strategies in each scenario. The results show that ALQC can effectively adapt to different operating conditions and system dynamics, thus maintaining cost-effectiveness in all scenarios.

Fig. 5 depicts the aggregrated TCLs power for one of the simulated districts with various reference power under ALQC demand response. The figures show that by adjusting $\Delta T_{\text{set}}^{\text{zone}}$ and $\Delta T_{\text{set}}^{\text{tank}}$, one can make the power y track the different levels of y_d. Let us recall that the noisy fluctuations around the desired values are due to the heterogeneity of the district. As compared to the large fluctuations in Fig. 3c, the control can reduce but not eliminate the noise (recall that large fluctuations in Fig. 3c are also caused by weather conditions, which are sensibly reduced in Fig. 5). Overall, the power tracking is

TABLE IV: Total costs across three districts with various reference power ($y_d = 0.32, 0.35, 0.38$, and piecewise) under different DR programs: PID, LQC, ALQC (proposed).

District	y_d	PID	LQC	ALQC
1	0.32	1.227	1.230	**1.222**
	0.35	0.740	0.752	**0.727**
	0.38	0.879	0.880	**0.871**
	piecewise	0.818	0.815	**0.789**
2	0.32	1.060	1.064	**1.057**
	0.35	0.715	0.717	**0.692**
	0.38	1.059	1.053	**1.050**
	piecewise	0.769	0.772	**0.754**
3	0.32	1.341	1.342	**1.339**
	0.35	0.805	0.811	**0.801**
	0.38	0.801	0.807	**0.800**
	piecewise	0.862	0.873	**0.848**

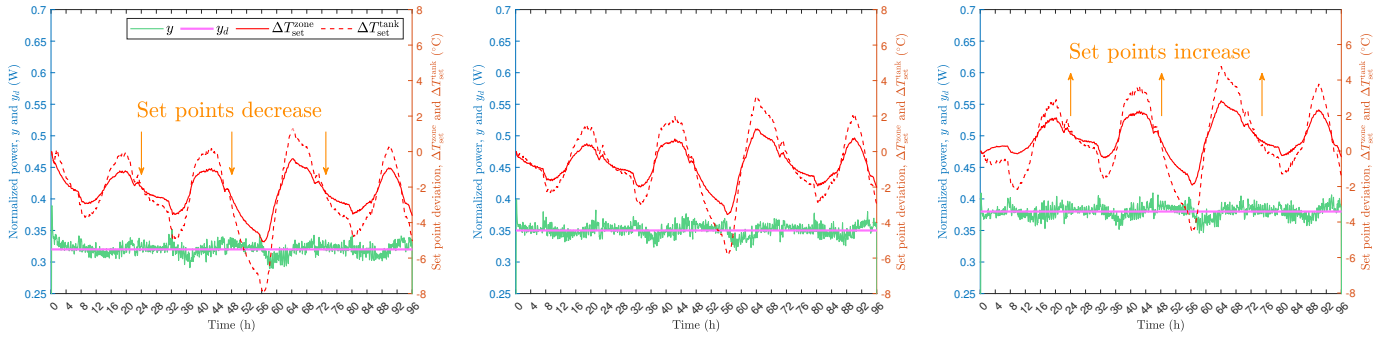

(a) $y_d = 0.32$ (b) $y_d = 0.35$ (c) $y_d = 0.38$

Fig. 5: Aggregated TCLs power y for one of the simulated districts with various reference power y_d under ALQC demand response: (a) $y_d = 0.32$; (b) $y_d = 0.35$; (c) $y_d = 0.38$. Case (a) and (c) represent a 3% power decrease and 3% power increase, respectively, as compared to case (b), which is consistent with practical DR programs. Note that the 3% power decrease in case (a) involves smaller $\Delta T_{\text{set}}^{\text{zone}}$ and $\Delta T_{\text{set}}^{\text{tank}}$ as compared to case (b). Meanwhile, the 3% power increase in case (c) involves larger $\Delta T_{\text{set}}^{\text{zone}}$ and $\Delta T_{\text{set}}^{\text{tank}}$. The noise is caused by the heterogeneity of the TCLs and buildings. Similar results occur also for other simulated districts (cf. Table IV) and are not reported for compactness.

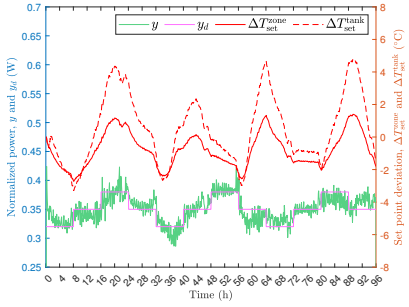

Fig. 6: Aggregated TCLs power y for one of the simulated districts with piecewise reference power y_d under ALQC demand response. Despite the noisy fluctuations caused by the heterogeneity of the TCLs and buildings, it is possible to track different power levels.

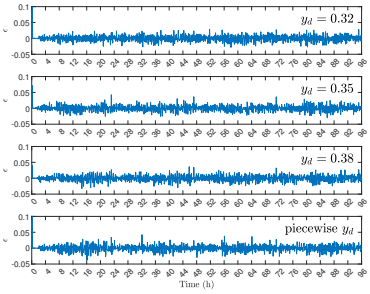

Fig. 7: Estimation error ε for one of the simulated districts with various reference power y_d ($y_d = 0.32, 0.35, 0.38$ and piecewise) under ALQC demand response. Notably, the estimation performance is consistent in all scenarios.

feasible and the set point deviations are also in reasonable ranges ±4 °C for the zone and ±8 °C for the tank. One can notice that, as compared to $y_d = 0.35$, the tracking of $y_d = 0.38$ is achieved by increasing the set point, whereas tracking $y_d = 0.32$ requires to lower the set points (which is reasonable in a heating scenario).

To confirm the tracking capabilities, we also show the performance under a piecewise constant y_d in Fig. 6: despite the noisy fluctuations, it is possible to track different power levels. The estimators with the proposed parametric model show good performance in each scenario, cf. the small estimation error ε in Fig. 7. Notably, although each district may differ in terms of building structure, usage patterns, and environmental conditions, the DR program show significant consistency. Finally, Fig. 8 separates y as y_{SH} and y_{HWST}: this is done in order to verify that the space heating units contribute to coarse regulation of the power consumption, whereas the tank units contribute to finer regulation.

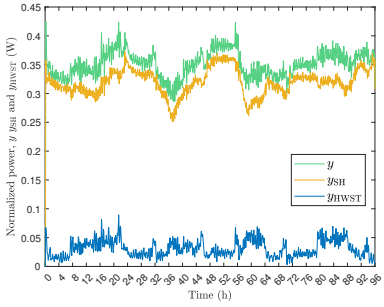

Fig. 8: Aggregated TCLs power y (in green), separated as space heating consumption y_{SH} (in yellow) and hot water storage tank consumption y_{HWST} (in blue) for one of the simulated districts for piecewise reference power y_d under ALQC demand response. It can be seen that space heating units allow coarse regulation of the power consumption, while the tank units contribute to finer regulation.

VIII. Conclusion and Future Work

Through extensive district simulators with heterogeneous buildings of different typologies (light-weight, nearly-zero energy, massive passive), we have shown the feasibility of controlling heterogeneous types of thermostatically controlled loads (TCLs) for shaping the power consumption of districts. We considered TCLs with not only different parameters, but also of different type (heating units, air conditioner units, boiler units). We have verified that, with a properly designed

demand response program, power tracking is possible, despite the large heterogeneity of the district. Optimality and adaptation of the demand response program have been studied analytically in the framework of adaptive linear quadratic control. Interestingly, different types of TCLs can serve different tasks, e.g., coarse regulation and finer regulation. We believe this provides an interesting connection with dual-stage actuators [37], i.e., actuators with a stage used for coarse regulation and another stage used for finer regulation.

APPENDIX A
PROOF OF THEOREM 1

Proof: Consider the observable canonical state-space form (15) with matrices as in (16). Because $R_p(z)$ is coprime to $Z_{q,1}(z)$ and $Z_{q,2}(z)$, then (A, B) is stabilizable.

Let $\boldsymbol{x}_o(k) \triangleq \boldsymbol{x}(k) - \hat{\boldsymbol{x}}(k)$ be the state-observation error. Substracting (25) from (15) and using (24) in (25), we obtain

$$\begin{bmatrix} \boldsymbol{x}_o(k+1) \\ \hat{\boldsymbol{x}}(k+1) \end{bmatrix} = \begin{bmatrix} A - K_o C^\top & \mathbf{0} \\ K_o C^\top & A - BK \end{bmatrix} \begin{bmatrix} \boldsymbol{x}_o(k) \\ \hat{\boldsymbol{x}}(k) \end{bmatrix}. \tag{29}$$

Since the eigenvalues of the state matrix in (29) are the eigenvalues of $A - K_o C^\top$, and of $A - BK$, where $A - K_o C^\top$ is a stable matrix by design, it follows that the origin of (29) is exponentially stable if and only if $A - BK$ is a stable matrix. So, consider

$$\breve{\boldsymbol{x}}(k+1) = (A - BK)\breve{\boldsymbol{x}}(k) \tag{30}$$

and we aim to prove that its origin is exponentially stable. Using (24) and $Q = CC^\top$, let us manipulate the Riccati equation (20) as

$$\begin{aligned} P &= A^\top PA - (A^\top PB)(B^\top PB + R)^{-1}(B^\top PB + R) \\ &\quad (B^\top PB + R)^{-1}(B^\top PA) + Q \\ &= A^\top PA - K^\top (B^\top PB + R)K + Q \\ &= (A - BK)^\top P(A - BK) + K^\top B^\top PA + A^\top PBK \\ &\quad - K^\top B^\top PBK - K^\top (B^\top PB + R)K + Q \\ &= (A - BK)^\top P(A - BK) + 2K^\top (B^\top PB + R)K \\ &\quad - K^\top B^\top PBK - K^\top (B^\top PB + R)K + Q \\ &= (A - BK)^\top P(A - BK) + K^\top RK + CC^\top. \end{aligned}$$

Choose the Lyapunov function

$$V(k) = \breve{\boldsymbol{x}}^\top(k) P \breve{\boldsymbol{x}}(k)$$

and compute the change of V along the trajectory of (30)

$$\begin{aligned} \Delta V(k) &= \breve{\boldsymbol{x}}^\top(k+1) P \breve{\boldsymbol{x}}(k+1) - \breve{\boldsymbol{x}}^\top(k) P \breve{\boldsymbol{x}}(k) \\ &= \breve{\boldsymbol{x}}^\top(k)(A - BK)^\top P(A - BK)\breve{\boldsymbol{x}}(k) - \breve{\boldsymbol{x}}^\top(k) P \breve{\boldsymbol{x}}(k) \\ &= \breve{\boldsymbol{x}}^\top(k)[(A - BK)^\top P(A - BK) - P]\breve{\boldsymbol{x}}(k) \\ &= -\breve{\boldsymbol{x}}^\top(k) C^\top C \breve{\boldsymbol{x}}(k) - \breve{\boldsymbol{x}}^\top(k) K^\top RK \breve{\boldsymbol{x}}(k) \leq 0 \end{aligned}$$

which implies that the origin of (30) is stable. Since

$$(A - BK)^\top P(A - BK) - P = -\begin{bmatrix} C^\top \\ R^{\frac{1}{2}} K \end{bmatrix}^\top \begin{bmatrix} C^\top \\ R^{\frac{1}{2}} K \end{bmatrix},$$

according to [34, Thm. A.12.22], if $\left(A - BK, \begin{bmatrix} C^\top \\ R^{\frac{1}{2}} K \end{bmatrix}\right)$ is observable, then the origin of (30) is exponentially stable.

Rewrite R as $R = (R^{\frac{1}{2}})^\top R^{\frac{1}{2}}$. Then $|R^{\frac{1}{2}}| \neq 0$, so that $B = MR^{\frac{1}{2}}$ for some M. Therefore, we have

$$\begin{aligned} \operatorname{rank} \begin{bmatrix} zI - A \\ C^\top \\ R^{\frac{1}{2}} K \end{bmatrix} &= \operatorname{rank} \begin{bmatrix} I & 0 & M \\ 0 & I & 0 \\ 0 & 0 & I \end{bmatrix} \begin{bmatrix} zI - A \\ C^\top \\ R^{\frac{1}{2}} K \end{bmatrix} \\ &= \operatorname{rank} \begin{bmatrix} zI - (A - BK) \\ C^\top \\ R^{\frac{1}{2}} K \end{bmatrix}. \end{aligned}$$

Since $(C^\top, A)$ is observable thanks to the observable canonical form (15), then by the Popov-Belevitch-Hautus rank tests [38, Thm. 2.4-9], $\operatorname{rank} \begin{pmatrix} zI - A \\ C^\top \end{pmatrix} = 3$ for every z, so that $\left(A - BK, \begin{bmatrix} C^\top \\ R^{\frac{1}{2}} K \end{bmatrix}\right)$ is observable. It follows that the origin of (30) is exponentially stable.

Therefore, the origin of (29) is exponentially stable. It follows that $\boldsymbol{x}_o(k), \hat{\boldsymbol{x}}(k) \in \ell_\infty$ and converge to $\mathbf{0}$ as k goes to ∞. From $\boldsymbol{x}_o = \boldsymbol{x} - \hat{\boldsymbol{x}}$, $e(k) = C^\top \boldsymbol{x}(k)$ and $\Delta \boldsymbol{T}_{\mathbf{set}}(k) = -K\hat{\boldsymbol{x}}(k)$, it follows that all closed-loop signal are bounded and $e(k)$ converges to 0 as k goes to ∞.

This completes the proof of Theorem 1. □

APPENDIX B
PROOF OF THEOREM 2

Proof: The proof is organized according to the following four steps: first, write the tracking error dynamics as a homogeneous term perturbed by estimation error terms; second, prove that the homogeneous term is exponentially stable; third, prove that the tracking error and other closed-loop signals of interest can be bounded using the estimation errors; fourth, using the norm-boundedness properties of the estimation errors, prove that the closed-loop signals are norm-bounded and the tracking error converges to zero.

Step 1. Calculate the closed-loop state error dynamics.

Consider the observable canonical state-space form (15) with matrices as in (16), let $\boldsymbol{x}_o(k) \triangleq \boldsymbol{x}(k) - \hat{\boldsymbol{x}}(k)$ be the state observation error. The relation between the tracking error and the state observation error, and between the tracking error and the inputs can be written respectively as

$$e(k) = C^\top \boldsymbol{x}_o(k) + C^\top \hat{\boldsymbol{x}}(k), \tag{31}$$

$$e(k) = \frac{\hat{Z}_{q,1}(k)}{\hat{R}_p(k)} \Delta T_{\text{set}}^{\text{zone}}(k) + \frac{\hat{Z}_{q,2}(k)}{\hat{R}_p(k)} \Delta T_{\text{set}}^{\text{tank}}(k). \tag{32}$$

From (15), (16) and (26)-(27), we have

$$\begin{aligned} \begin{bmatrix} \boldsymbol{x}_o(k+1) \\ \hat{\boldsymbol{x}}(k+1) \end{bmatrix} &= \begin{bmatrix} A_o & \mathbf{0} \\ \hat{K}_o(k) C^\top & A_c(k) \end{bmatrix} \begin{bmatrix} \boldsymbol{x}_o(k) \\ \hat{\boldsymbol{x}}(k) \end{bmatrix} \\ &+ \begin{bmatrix} -\tilde{\boldsymbol{\theta}}_{q,1}(k) & -\tilde{\boldsymbol{\theta}}_{q,2}(k) \\ \mathbf{0} & \mathbf{0} \end{bmatrix} \Delta \boldsymbol{T}_{\mathbf{set}}(k) + \begin{bmatrix} \tilde{\boldsymbol{\theta}}_p(k) \\ \mathbf{0} \end{bmatrix} e(k), \end{aligned} \tag{33}$$

where $A_o \triangleq \left[\begin{array}{c|c} -\boldsymbol{p}^* & \frac{I_2}{0} \end{array}\right]$ is a stable matrix,

$$\begin{aligned} A_c(k) &\triangleq \hat{A}(k) - \hat{B}(k)\hat{K}(k), \\ \tilde{\boldsymbol{\theta}}_p(k) &\triangleq \boldsymbol{\theta}_p(k) - \boldsymbol{\theta}_p^* = [-\tilde{a}_{1d} \;\; -\tilde{a}_{2d} \;\; 0]^\top, \\ \tilde{\boldsymbol{\theta}}_{q,1}(k) &\triangleq \boldsymbol{\theta}_{q,1}(k) - \boldsymbol{\theta}_{q,1}^* = [\tilde{b}_1 \;\; \tilde{b}_2 \;\; \tilde{b}_3]^\top, \\ \tilde{\boldsymbol{\theta}}_{q,2}(k) &\triangleq \boldsymbol{\theta}_{q,2}(k) - \boldsymbol{\theta}_{q,2}^* = [\tilde{c}_1 \;\; \tilde{c}_2 \;\; \tilde{c}_3]^\top, \end{aligned}$$

and where we have used the fact that

$$\begin{bmatrix} e & 1 & 0 \\ f & 0 & 1 \\ g & 0 & 0 \end{bmatrix}\begin{bmatrix} q \\ r \\ s \end{bmatrix} = \begin{bmatrix} e \\ f \\ g \end{bmatrix} C^\top \begin{bmatrix} q \\ r \\ s \end{bmatrix} + \begin{bmatrix} r \\ s \\ 0 \end{bmatrix}.$$

Step 2. Establish the exponential stability of the homogeneous part of (33).

When $\hat{R}_p(z,k)$ is strongly coprime to $\hat{Z}_{q,1}(z,k)$ and $\hat{Z}_{q,2}(z,k)$ at each time k, then $(\hat{A}(k),\hat{B}(k))$ is always stabilizable, and we can establish that $P(k),\hat{K}(k) \in \ell_\infty$. In addition, $\hat{A}(k),\hat{B}(k) \in \ell_\infty$ due to the properties of the adaptive law in Lemma 1. Also, $\Delta\hat{A}(k) \in \ell_2$ is guaranteed by the adaptive law. The following manipulations hold

$$\begin{aligned}
&P(k+2) - P(k+1) - \big(\hat{A}(k+1) - \hat{B}(k+1)\hat{K}(k+1)\big)^\top \\
&\big(P(k+1) - P(k)\big)\big(\hat{A}(k+1) - \hat{B}(k+1)\hat{K}(k+1)\big) \\
&= \hat{A}^\top(k+1)P(k)\hat{A}(k+1) - \hat{A}^\top(k)P(k)\hat{A}(k) \\
&\quad + \hat{K}^\top(k)R\hat{K}(k) + \hat{K}^\top(k+1)R\hat{K}(k+1) \\
&\quad - \hat{K}^\top(k+1)\hat{B}^\top(k+1)P(k)\hat{A}(k+1) \\
&\quad - \hat{A}^\top(k+1)P(k)\hat{B}(k+1)\hat{K}(k+1) \\
&\quad + \hat{K}^\top(k)\hat{B}^\top(k)P(k)\hat{B}(k)\hat{K}(k) \\
&\quad + \hat{K}^\top(k+1)\hat{B}^\top(k+1)P(k)\hat{B}(k+1)\hat{K}(k+1),
\end{aligned}$$

where we have used the fact that

$$\begin{aligned}
\hat{K}^\top(k)\big(\hat{B}^\top(k)P(k)\hat{B}(k) + R\big) &= \hat{A}^\top(k)P(k)\hat{B}(k), \\
\hat{K}^\top(k)\big(\hat{B}^\top(k)P(k)\hat{B}(k) + R\big)\hat{K}(k) &= \hat{K}^\top(k)\hat{B}^\top(k)P(k)\hat{A}(k).
\end{aligned}$$

It follows from $P(k),\hat{K}(k),\hat{A}(k),\hat{B}(k) \in \ell_\infty$ that

$$\begin{aligned}
&P(k+2) - P(k+1) - \big(\hat{A}(k+1) - \hat{B}(k+1)\hat{K}(k+1)\big)^\top \\
&\big(P(k+1) - P(k)\big)\big(\hat{A}(k+1) - \hat{B}(k+1)\hat{K}(k+1)\big) \in \ell_\infty.
\end{aligned}$$

Let us decompose $P(k)$ as $P(k) = S^\top(k)S(k)$. From the fact that

$$\begin{aligned}
&\hat{K}^\top(k)\hat{B}^\top(k)P(k)\hat{B}(k)\hat{K}(k) \in \ell_\infty, \\
&\hat{K}^\top(k+1)\hat{B}^\top(k+1)P(k)\hat{B}(k+1)\hat{K}(k+1) \in \ell_\infty,
\end{aligned}$$

we can establish

$$S(k)\hat{B}(k)\hat{K}(k),\ S(k)\hat{B}(k+1)\hat{K}(k+1) \in \ell_\infty \cap \ell_2.$$

From $A_c(k) = \hat{A}(k) - \hat{B}(k)\hat{K}(k)$, we obtain

$$\begin{aligned}
\|\Delta A_c(k)\|_2 =& \|\hat{A}(k+1) - S^{-1}(k)S(k)\hat{B}(k+1)\hat{K}(k+1) \\
&- \hat{A}(k) + S^{-1}(k)S(k)\hat{B}(k)\hat{K}(k)\|_2 \\
\le& \|\Delta\hat{A}(k)\|_2 + \|S^{-1}(k)\|_2\|S(k)\hat{B}(k)\hat{K}(k)\|_2 \\
&+ \|S^{-1}(k)\|_2\|S(k)\hat{B}(k+1)\hat{K}(k+1)\|_2. \quad (34)
\end{aligned}$$

It follows from (34) that $\Delta A_c(k) \in \ell_2$. Because $A_c(k)$ is a stable matrix at each time k, we can conclude that $A_c(k)$ is uniformly asymptotically stable. Also, as A_o is a stable matrix, the homogeneous part of (33) is exponentially stable.

Step 3. Use the properties of $\ell_{2\delta}$ norm and the discrete-time Bellman-Gronwall lemma to establish boundedness.

From (31), (32) and (33), we obtain the following bounds

$$\|\hat{\boldsymbol{x}}_k\|_{2\delta} \le c\|C^\top \boldsymbol{x}_{o_k}\|_{2\delta}, \quad (35)$$

$$\|e_k\|_{2\delta} \le c\|C^\top \boldsymbol{x}_{o_k}\|_{2\delta} + c\|\hat{\boldsymbol{x}}_k\|_{2\delta} \le c\|C^\top \boldsymbol{x}_{o_k}\|_{2\delta}, \quad (36)$$

$$\|\Delta T^{\text{zone}}_{\text{set}_k}\|_{2\delta},\ \|\Delta T^{\text{tank}}_{\text{set}_k}\|_{2\delta} \le c\|e_k\|_{2\delta} \le c\|C^\top \boldsymbol{x}_{o_k}\|_{2\delta}, \quad (37)$$

for some constant $c > 0$. We relate the term $C^\top \boldsymbol{x}_o(k)$ with the estimation error by using (33) to express $C^\top \boldsymbol{x}_o(k)$ as

$$\begin{aligned}
C^\top \boldsymbol{x}_o(k) = C^\top\big(zI - A_o\big)^{-1}\big(&\tilde{\boldsymbol{\theta}}_p(k)e(k) - \tilde{\boldsymbol{\theta}}_{q,1}(k)\Delta T^{\text{zone}}_{\text{set}}(k) \\
&- \tilde{\boldsymbol{\theta}}_{q,2}(k)\Delta T^{\text{tank}}_{\text{set}}(k)\big).
\end{aligned}$$

Noting that (C, A_o) is in the observer canonical form, i.e. $C^\top\big(zI - A_o\big)^{-1} = \dfrac{\bar{\boldsymbol{\alpha}}^\top(z)}{A_o^*(z)}$, with $A_o^*(z) = \det\big(zI - A_o\big)$, we have

$$\begin{aligned}
C^\top \boldsymbol{x}_o(k) = &-\sum_{v=1}^{2} \frac{z^{3-v}}{A_o^*(z)}\tilde{a}_{vd}(k)e(k) \\
&- \sum_{v=1}^{3} \frac{z^{3-v}}{A_o^*(z)}\Big(\tilde{b}_v(k)\Delta T^{\text{zone}}_{\text{set}}(k) + \tilde{c}_v(k)\Delta T^{\text{tank}}_{\text{set}}(k)\Big).
\end{aligned}$$

Let us denote $\Lambda_p(z) = z^3 + \boldsymbol{\lambda}_p^\top\bar{\boldsymbol{\alpha}}(z)$, with $\boldsymbol{\lambda}_p = [\lambda_2, \lambda_1, \lambda_0]^\top$ a Hurwitz polynomial. Applying the discrete-time swapping lemma [34, Lem. A.12.35] with $W(z) = \dfrac{z^{3-v}}{\Lambda_p(z)}$ to each term under the summation, we have

$$\begin{aligned}
\frac{z^{3-v}}{A_o^*(z)}\tilde{a}_{vd}(k)e(k) = \frac{\Lambda_p(z)}{A_o^*(z)}\Bigg(&\tilde{a}_{vd}(k)\frac{z^{3-v}}{\Lambda_p(z)}e(k) \\
&+ W_{c_v}(z)\big(W_{b_v}(z)e(k)\big)\Delta\tilde{a}_{vd}(k)\Bigg),
\end{aligned}$$

where $W_{c_v}(z)$, $W_{b_v}(z)$ are strictly proper transfer functions, having the same poles as $\dfrac{1}{\Lambda_p(z)}$, and similar for the terms with $\Delta T^{\text{zone}}_{\text{set}}(k)$ and $\Delta T^{\text{tank}}_{\text{set}}(k)$. Therefore, $C^\top \boldsymbol{x}_o(k)$ can be expressed as

$$\begin{aligned}
C^\top \boldsymbol{x}_o(k) &= r_1(k) + \frac{\Lambda_p(z)}{A_o^*(z)}\Bigg[-\sum_{v=1}^{2}\tilde{a}_{vd}(k)\frac{z^{3-v}}{\Lambda_p(z)}e(k) \\
&- \sum_{v=1}^{3}\left(\tilde{b}_v(k)\frac{z^{3-v}}{\Lambda_p(z)}\Delta T^{\text{zone}}_{\text{set}}(k) + \tilde{c}_v(k)\frac{z^{3-v}}{\Lambda_p(z)}\Delta T^{\text{tank}}_{\text{set}}(k)\right)\Bigg] \\
&= r_1(k) + \frac{\Lambda_p(z)}{A_o^*(z)}\Bigg(\tilde{\boldsymbol{\theta}}_p^\top(k)\frac{\bar{\boldsymbol{\alpha}}(z)}{\Lambda_p(z)}e(k) \\
&- \tilde{\boldsymbol{\theta}}_{q,1}^\top(k)\frac{\bar{\boldsymbol{\alpha}}(z)}{\Lambda_p(z)}\Delta T^{\text{zone}}_{\text{set}}(k) - \tilde{\boldsymbol{\theta}}_{q,2}^\top(k)\frac{\bar{\boldsymbol{\alpha}}(z)}{\Lambda_p(z)}\Delta T^{\text{tank}}_{\text{set}}(k)\Bigg), \quad (38)
\end{aligned}$$

where

$$\begin{aligned}
r_1(k) \triangleq \frac{\Lambda_p(z)}{A_o^*(z)}\Bigg[&-\sum_{v=1}^{2} W_{c_v}(z)\big(W_{b_v}(z)e(k)\big)\Delta\tilde{a}_{vd}(k) \\
&- \sum_{v=1}^{3} W_{c_v}(z)W_{b_v}(z)\Big(\Delta T^{\text{zone}}_{\text{set}}(k)\Delta\tilde{b}_v(k) \\
&+ \Delta T^{\text{tank}}_{\text{set}}(k)\Delta\tilde{c}_v(k)\Big)\Bigg].
\end{aligned}$$

We now note that (32) can be rewritten as

$$\hat{\zeta}(k) = \boldsymbol{\theta}^\top(k)\boldsymbol{\Phi}(k),$$

where

$$\hat{\zeta}(k) = \frac{z^3}{\Lambda_p(z)}e(k),\ \boldsymbol{\theta}(k) = [\boldsymbol{\theta}_{q,1}^\top(k)\ \boldsymbol{\theta}_{q,2}^\top(k)\ \boldsymbol{\theta}_p^\top(k)]^\top,$$
$$\boldsymbol{\Phi}(k) = \frac{\bar{\boldsymbol{\alpha}}^\top(z)}{\Lambda_p(z)}\begin{bmatrix}\Delta T_{\text{set}}^{\text{zone}}(k) & \Delta T_{\text{set}}^{\text{tank}}(k) & -e(k)\end{bmatrix}^\top$$
$$= [\boldsymbol{\phi}_1^\top(k)\ \ \boldsymbol{\phi}_2^\top(k)\ \ \boldsymbol{\phi}_3^\top(k)]^\top. \tag{39}$$

Using (39) and the discrete-time swapping lemma [34, Lem. A.12.35] in (38), we obtain

$$C^\top \boldsymbol{x}_o(k) = -\frac{\Lambda_p(z)}{A_o^*(z)}\tilde{\boldsymbol{\theta}}^\top(k)\boldsymbol{\Phi}(k) + r_1(k), \tag{40}$$

where $\tilde{\boldsymbol{\theta}}(k)$ is the estimation error of $\boldsymbol{\theta}(k)$ in (39).

The normalized estimation error satisfies the equation

$$-\tilde{\boldsymbol{\theta}}^\top(k)\boldsymbol{\Phi}(k) = -\big(\tilde{\boldsymbol{\theta}}^\top(k-1) + \varepsilon(k)\boldsymbol{\Phi}^\top(k)P_1(k)\big)\boldsymbol{\Phi}(k)$$
$$= \varepsilon(k)m^2(k)\left(1 - \frac{\boldsymbol{\Phi}^\top(k)P_1(k)\boldsymbol{\Phi}(k)}{m^2(k)}\right),$$

which can be used in (40) to obtain

$$C^\top \boldsymbol{x}_o(k) = \frac{\Lambda_p(z)}{A_o^*(z)}\varepsilon(k)m^2(k)\left(1-\frac{\boldsymbol{\Phi}^\top(k)P_1(k)\boldsymbol{\Phi}(k)}{m^2(k)}\right)+r_1(k). \tag{41}$$

Defining an auxiliary normalizing signal

$$m_f^2(k) \triangleq 1 + \|\Delta T_{\text{set}_k}^{\text{zone}}\|_{2\delta}^2 + \|\Delta T_{\text{set}_k}^{\text{tank}}\|_{2\delta}^2 + \|e_k\|_{2\delta}^2,$$

we have $\boldsymbol{\Phi}(k)/m_f(k), m(k)/m_f(k) \in \ell_\infty$ for some $\delta > 0$. From the definition of $r_1(k)$ and $\left|1-\frac{\boldsymbol{\Phi}^\top(k)P_1(k)\boldsymbol{\Phi}(k)}{m^2(k)}\right| < 1$, we obtain

$$\|C^\top \boldsymbol{x}_{o_k}\|_{2\delta} \le c\|\varepsilon_k m_k^2\|_{2\delta} + c\left\|\sum_{v=1}^{2}\Delta\tilde{a}_{vd_k}e_k\right\|_{2\delta}$$
$$+ c\left\|\sum_{v=1}^{3}\Delta\tilde{b}_{v_k}\Delta T_{\text{set}_k}^{\text{zone}}\right\|_{2\delta} + c\left\|\sum_{v=1}^{3}\Delta\tilde{c}_{v_k}\Delta T_{\text{set}_k}^{\text{tank}}\right\|_{2\delta}. \tag{42}$$

Using (42) in (36)-(37) and the properties of $m_f(k)$, we have the following inequality:

$$m_f^2(k) \le c\|g_k m_{f_k}\|_{2\delta}^2 + c,$$

where

$$g^2(k) \triangleq \varepsilon^2(k)m^2(k) + \left|\sum_{v=1}^{2}\Delta\tilde{a}_{vd}(k)\right|^2$$
$$+ \left|\sum_{v=1}^{3}\Delta\tilde{b}_v(k)\right|^2 + \left|\sum_{v=1}^{3}\Delta\tilde{c}_v(k)\right|^2$$

and $g \in \ell_2$ due to the properties of the adaptive law in Lemma 1. If we now apply the Bellman-Gronwall lemma [34, Lem. A.6.3] to the above inequality we can show that $m_f(k) \in \ell_\infty$. From $m_f(k) \in \ell_\infty$ and the properties of the $\ell_{2\delta}$ norm we can establish boundness for the rest of the closed-loop signals.

Step 4. Convergence of the error to zero.

Since all closed-loop signals are bounded, we can establish that $\Delta(\varepsilon(k)m^2(k)) \in \ell_\infty$, which, together with $\varepsilon(k)m^2(k) \in \ell_\infty \cap \ell_2$, implies that $\varepsilon(k)m^2(k)$ converges to 0, and therefore, $\Delta\boldsymbol{\theta}(k)$ converges to $\mathbf{0}$ as k goes to ∞. From the expression of $r_1(k)$ we can conclude that $r_1(k) \in \ell_2$ and converges to 0 as k goes to ∞. Using $\varepsilon(k)m^2(k), r_1(k) \in \ell_2$ and convergence of $r_1(k)$ in (41), we have that $C^\top \boldsymbol{x}_o(k) \in \ell_2$ and converges to 0 as k goes to ∞.

Consider (33), since $A_c(k)$ is uniformly asymptotically stable, and $C^\top \boldsymbol{x}_o(k) \in \ell_2$ and convergent we get that $\hat{\boldsymbol{x}}(k)$ converges to 0 as k goes to ∞. From $e(k) = C^\top \boldsymbol{x}_o(k) + C^\top \hat{\boldsymbol{x}}(k)$, it follows that $e(k)$ converges to 0 as k goes to ∞.

This completes the proof of Theorem 2. □

REFERENCES

[1] A. Kleidaras, A. E. Kiprakis, and J. S. Thompson, "Human in the loop heterogeneous modelling of thermostatically controlled loads for demand side management studies," *Energy*, vol. 145, pp. 754–769, 2018.

[2] E. C. Kara, M. D. Tabone, J. S. MacDonald, D. S. Callaway, and S. Kiliccote, "Quantifying flexibility of residential thermostatically controlled loads for demand response: A data-driven approach," *BuildSys 2014 - Proceedings of the 1st ACM Conference on Embedded Systems for Energy-Efficient Buildings*, pp. 140–147, 2014.

[3] G. Tian and Q. Z. Sun, "A stochastic controller for primary frequency regulation using on/off demand side resources," *IEEE Transactions on Smart Grid*, vol. 14, no. 5, pp. 4141–4144, 2023.

[4] A. Kasis and I. Lestas, "Frequency regulation with thermostatically controlled loads: Aggregation of dynamics and synchronization," *IEEE Transactions on Automatic Control*, vol. 67, no. 10, pp. 5602–5609, 2022.

[5] M. Shad, A. Momeni, R. Errouissi, C. P. Diduch, M. E. Kaye, and L. Chang, "Identification and estimation for electric water heaters in direct load control programs," *IEEE Transactions on Smart Grid*, vol. 8, no. 2, pp. 947–955, 2017.

[6] J. Hu, J. Cao, T. Yong, J. M. Guerrero, M. Z. Q. Chen, and Y. Li, "Demand response load following of source and load systems," *IEEE Transactions on Control Systems Technology*, vol. 25, no. 5, pp. 1586–1598, 2017.

[7] D. Bauso, "Dynamic demand and mean-field games," *IEEE Transactions on Automatic Control*, vol. 62, no. 12, pp. 6310–6323, 2017.

[8] M. Chertkov and V. Chernyak, "Ensemble of thermostatically controlled loads: Statistical physics approach," *Scientific Reports*, vol. 7, no. 1, 2017.

[9] D. S. Callaway, "Tapping the energy storage potential in electric loads to deliver load following and regulation, with application to wind energy," *Energy Conversion & Management*, vol. 50, no. 5, pp. 1389–1400, 2009.

[10] E. Benenati, M. Colombino, and E. Dall'Anese, "A tractable formulation for multi-period linearized optimal power flow in presence of thermostatically controlled loads," in *2019 IEEE 58th Conference on Decision and Control (CDC)*, 2019, pp. 4189–4194.

[11] L. C. Totu, R. Wisniewski, and J. Leth, "Demand response of a TCL population using switching-rate actuation," *IEEE Transactions on Control Systems Technology*, vol. 25, no. 5, pp. 1537–1551, 2017.

[12] J. Zheng, G. Laparra, G. Zhu, and M. Li, "Aggregate power control of heterogeneous TCL populations governed by Fokker-Planck equations," *IEEE Transactions on Control Systems Technology*, vol. 28, no. 5, pp. 1915–1927, 2020.

[13] A. Ghaffari, S. Moura, and M. Krstic, "Analytic modeling and integral control of heterogeneous thermostatically controlled load populations," *ASME 2014 Dynamic Systems and Control Conference, DSCC 2014*, vol. 2, 2014.

[14] W. Zhang, K. Kalsi, J. Lian, and C.-Y. Chang, "Aggregated modeling and control of air conditioning loads for demand response," *IEEE Transactions on Power Systems*, vol. 28, no. 4, pp. 4655–4664, 2013.

[15] L. Zhao and W. Zhang, "A unified stochastic hybrid system approach to aggregate modeling of responsive loads," *IEEE Transactions on Automatic Control*, vol. 63, no. 12, pp. 4250–4263, 2018.

[16] S. Esmaeil Zadeh Soudjani and A. Abate, "Aggregation and control of populations of thermostatically controlled loads by formal abstractions," *IEEE Transactions on Control Systems Technology*, vol. 23, no. 3, pp. 975–990, 2015.

[17] F. A. C. C. Fontes, A. Halder, J. Becerril, and P. R. Kumar, "Optimal control of thermostatic loads for planning aggregate consumption: Characterization of solution and explicit strategies," *IEEE Control Systems Letters*, vol. 3, no. 4, pp. 877–882, 2019.

[18] G. Wang, Z. Li, and F. Wang, "Enhanced sufficient battery model for aggregate flexibility of thermostatically controlled loads considering coupling constraints," *IEEE Transactions on Sustainable Energy*, vol. 12, no. 4, pp. 2493–2496, 2021.

[19] X. Gong, E. Castillo-Guerra, J. L. Cardenas-Barrera, B. Cao, S. A. Saleh, and L. Chang, "Robust hierarchical control mechanism for aggregated thermostatically controlled loads," *IEEE Transactions on Smart Grid*, vol. 12, no. 1, pp. 453–467, 2021.

[20] M. Kaheni, A. Pilloni, G. S. Ruda, E. Usai, and M. Franceschelli, "Distributed asynchronous greedy control of large networks of thermostatically controlled loads for electric demand response," *IEEE Control Systems Letters*, vol. 7, pp. 169–174, 2023.

[21] Y. Wang, Y. Tang, Y. Xu, and Y. Xu, "A distributed control scheme of thermostatically controlled loads for the building-microgrid community," *IEEE Transactions on Sustainable Energy*, vol. 11, no. 1, pp. 350–360, 2020.

[22] M. Franceschelli, A. Pilloni, and A. Gasparri, "Multi-agent coordination of thermostatically controlled loads by smart power sockets for electric demand side management," *IEEE Transactions on Control Systems Technology*, vol. 29, no. 2, pp. 731–743, 2021.

[23] M. Kamgarpour, C. Ellen, S. E. Z. Soudjani, S. Gerwinn, J. L. Mathieu, N. Müllner, A. Abate, D. S. Callaway, M. Fränzle, and J. Lygeros, "Modeling options for demand side participation of thermostatically controlled loads," in *2013 IREP Symposium Bulk Power System Dynamics and Control*, 2013, pp. 1–15.

[24] S. Zou, Z. Chen, and J. Lygeros, "Price control for heterogeneous thermostatically controlled loads in communication and computation delay environments," in *2019 IEEE 58th Conference on Decision and Control (CDC)*, 2019, pp. 4453–4458.

[25] S. H. Tindemans and G. Strbac, "Low-complexity decentralized algorithm for aggregate load control of thermostatic loads," *IEEE Transactions on Industry Applications*, vol. 57, no. 1, pp. 987–998, 2021.

[26] J. Hu, J. Cao, M. Z. Q. Chen, J. Yu, J. Yao, S. Yang, and T. Yong, "Load following of multiple heterogeneous TCL aggregators by centralized control," *IEEE Transactions on Power Systems*, vol. 32, no. 4, pp. 3157–3167, 2017.

[27] S. Iacovella, F. Ruelens, P. Vingerhoets, B. Claessens, and G. Deconinck, "Cluster control of heterogeneous thermostatically controlled loads using tracer devices," *IEEE Transactions on Smart Grid*, vol. 8, no. 2, pp. 528–536, 2017.

[28] B. Vand, R. Ruusu, A. Hasan, and B. M. Delgado, "Optimal management of energy sharing in a community of buildings using a model predictive control," *Energy Conversion and Management*, vol. 239, p. 114178, 2021.

[29] S. Kilpeläinen, M. Lu, S. Cao, A. Hasan, and S. Chen, "Composition and operation of a semi-virtual renewable energy-based building emulator," *Future Cities and Environment*, vol. 4, no. 1, 2018.

[30] B. Manrique Delgado, R. Ruusu, A. Hasan, S. Kilpeläinen, S. Cao, and K. Sirén, "Energetic, cost, and comfort performance of a nearly-zero energy building including rule-based control of four sources of energy flexibility," *Buildings*, vol. 8, no. 12, p. 172, 2018.

[31] B. Cui, C. Fan, J. Munk, N. Mao, F. Xiao, J. Dong, and T. Kuruganti, "A hybrid building thermal modeling approach for predicting temperatures in typical, detached, two-story houses," *Applied Energy*, vol. 236, pp. 101–116, 2019.

[32] S. M. M. Rahman, "Simplified 3R-2C building thermal network model: A case study," *International Journal of Structural and Construction Engineering*, vol. 13, no. 6, pp. 288 – 294, 2019.

[33] Y. Zhang, B. Vand, and S. Baldi, "A review of mathematical models of building physics and energy technologies for environmentally friendly integrated energy management systems," *Buildings*, vol. 12, no. 2, 2022.

[34] P. A. Ioannou and B. Fidan, "Adaptive control tutorial," in *Advances in design and control*, 2006.

[35] X. Sun, H. Xie, Y. Xiao, and Z. Bie, "Incentive compatible pricing for enhancing the controllability of price-based demand response," *IEEE Transactions on Smart Grid*, vol. 15, no. 1, pp. 418–430, 2024.

[36] X. Chen, D. Liu, Y. Zhang, and S. Baldi, "Averaging thermal dynamics for nearly optimal and adaptive energy management of multi-zone homes," *IEEE Transactions on Consumer Electronics*, vol. 70, no. 1, pp. 4321–4332, 2024.

[37] S. Zhou and M. Tomizuka, "Enhanced anti-windup compensation for the dual stage hard disk drive systems with amplitude saturation," in *2016 IEEE International Conference on Advanced Intelligent Mechatronics (AIM)*, 2016, pp. 822–827.

[38] T. Kailath, *Linear systems*. Prentice-Hall Englewood Cliffs, NJ, 1980, vol. 156.